

# Poole Frenkel current and Schottky emission in SiN gate dielectric in AlGaIn/GaN metal insulator semiconductor heterostructure field effect transistors

Mina J. Hanna, Han Zhao, and Jack C. Lee

*Department of Electrical and Computer Engineering, The University of Texas at Austin, Texas 78758, USA*

(Received 22 February 2012; accepted 1 October 2012; published online 10 October 2012)

We analyze the anomalous I-V behavior in SiN prepared by plasma enhanced chemical vapor deposition for use as a gate insulator in AlGaIn/GaN metal insulator semiconductor heterostructure field effect transistors (HFETs). We observe leakage current across the dielectric with opposite polarity with respect to the applied electric field once the voltage sweep reaches a level below a determined threshold. This is observed as the absolute minimum of the leakage current does not occur at minimum voltage level (0 V) but occurs earlier in the sweep interval. Curve-fitting analysis suggests that the charge-transport mechanism in this region is Poole-Frenkel current, followed by Schottky emission due to band bending. Despite the current anomaly, the sample devices have shown a notable reduction of leakage current of over 2 to 6 order of magnitudes compared to the standard Schottky HFET. We show that higher pressures and higher silane concentrations produce better films manifesting less trapping. This conforms to our results that we reported in earlier publications. We found that higher chamber pressure achieves higher sheet carrier concentration that was found to be strongly dependent on the trapped space charge at the SiN/GaN interface. This would suggest that a lower chamber pressure induces more trap states into the SiN/GaN interface. © 2012 American Institute of Physics. [<http://dx.doi.org/10.1063/1.4758995>]

AlGaIn/GaN heterostructure field-effect transistors (HFETs) are extensively studied for their potentially superior performance for use in power devices. Their many attractive features<sup>1,2</sup> include high electron mobility and high velocity saturation, which are attributed to the carriers' generation at the AlGaIn/GaN interface leading to the formation of a two-dimensional electron gas (2DEG). To reduce gate leakage currents caused by the low Schottky barrier height, defects in the material, and the metal/AlGaIn interface, the gate Schottky contact is often replaced with a metal-insulator-semiconductor (MIS) structure.<sup>1,2</sup> The performance of these devices is largely determined by the quality of the dielectric, limited by its complex mechanisms of charge transport, its trapping defects, and other imperfections, which depend on the synthesis technique of the film.

Different dielectrics have been used for this purpose, including SiO<sub>2</sub>,<sup>1,3</sup> Al<sub>2</sub>O<sub>3</sub>,<sup>4,5</sup> HfO<sub>2</sub>,<sup>6</sup> and SiN.<sup>3,7,8</sup> Each material has several merits recorded in literature as well as limitations for the device performance.<sup>9,10</sup>

SiN grown by plasma enhanced chemical vapor deposition (PECVD) can contain a high density of localized trap states due to structural disorder and defects, such as silicon dangling bonds and Si-Si bonds, which are caused by random misalignments of atoms with respect to bonding angles.<sup>11,12</sup> This is in addition to complex radicals based on [Si-H] and [N-H] bonding groups. It was shown that Poole-Frenkel (PF) and Fowler-Nordheim (FN) currents constitute the SiN leakage current in high fields (above ~2 MV/cm).<sup>12,13</sup> Additionally, PF currents were found to dominate in nearly stoichiometric SiN compositions.<sup>13</sup> In low fields, Schottky currents and ohmic conduction are believed to dominate.<sup>14,15</sup> In this paper, we analyze the current-voltage characteristics in SiN that potentially

contains a high density of bulk traps and examine how this correlates with the PECVD growth conditions.

We implement the design of experiment (DOE) methodology<sup>16</sup> and use statistical analysis to determine the effect of varying one or more parameters of the deposition process on the SiN film properties. Eight different permutations of three PECVD input parameters are shown in Table I. The constant RF power is kept constant in order to limit the number of permutations. Ellipsometry measurements were used to keep the film thickness as nearly constant as possible in all the experiments.

We used an OXFORD Plasma Lab 80 with a 13.56 MHz RF source at a constant power of 15 W. The precursor gases were silane (SiH<sub>4</sub>, 2% diluted in N<sub>2</sub>) and ammonia (NH<sub>3</sub>). The samples consisted of metal-insulator-metal (MIM) capacitor arrays on a (100) p-type Si substrate with doping of the order of 10<sup>16</sup> cm<sup>-3</sup>, coated with 360 nm of SiO<sub>2</sub> by PECVD (*n* = 1.46). The contacts consisted of a 20-nm Ti layer, evaporated by e-beam, followed by a 50-nm thermally evaporated Au layer.

SiN films were also deposited onto AlGaIn/GaN to form large-area MIS diodes (Table II). The epitaxial layer structure, grown by metal organic chemical vapor deposition (MOCVD) on a 100 mm (111)-oriented Si substrate (Nitronex Corp.), consisted of an undoped 18-nm Al<sub>0.26</sub>Ga<sub>0.74</sub>N layer on a GaN/transition layer stack, capped with a thin (~2 nm) GaN layer. Prior to the SiN deposition, all samples were cleaned using oxygen plasma in a barrel reactor with 350 sccm O<sub>2</sub> gas with a 100-W RF power at 13.56 MHz. They were then immersed in HCl:H<sub>2</sub>O (1:1) solution for 60 s. One sample was left without SiN to serve as a reference. Finally, Ni/Au (50 nm/200 nm) gates were evaporated using an electron beam and thermal energy, respectively. We

TABLE I. Complete set of PECVD parameters used in this experiment. The RF power was fixed at 15 W.

Sample	Temperature [°C]	Pressure [mTorr]	SiH <sub>4</sub> -NH <sub>3</sub> flow [sccm]	Time [min: s]	Thickness [nm]	Refractive index	Shift [V]
1	350	650	36–29	2:03	9.76	1.85	0.95
2	350	650	17–50	4:35	8.46	1.80	2.65
3	350	250	36–29	2:10	9.72	1.79	1.975
4	350	250	17–50	5:10	9.48	1.81	1.25
5	250	650	36–29	1:40	8.66	1.81	1
6	250	650	17–50	4:10	9.96	1.85	3
7	250	250	36–29	2:00	9.27	1.80	2.05
8	250	250	17–50	4:30	9.21	1.79	1.35

previously reported their transport properties.<sup>17</sup> The first step in the MIS diode fabrication (samples A-C) is mesa isolation, performed by inductively coupled plasma (ICP) dry etching using BCl<sub>3</sub>/Ar chemistry. Ohmic contacts consisting of a Ti/Al/Ni/Au (15/100/40/50 nm) metal stack were deposited by e-beam evaporation and subsequently annealed at 825 °C for 30 s in N<sub>2</sub> ambience. Subsequently, ~12 nm of SiN were deposited using three different PECVD protocols (see Table II). Finally, Ni/Au (50/200 nm) was evaporated as a gate contact for circular diodes ( $A = 7.854 \times 10^{-5} \text{ cm}^2$ ).

Figure 1 illustrates the I-V behavior of the MIM samples grown on SiO<sub>2</sub>/Si substrates. The curves denote the absolute value of the current measured while sweeping the voltage from -5 V to +5 V (curve 1) and conversely from +5 V to -5 V (curve 2). We found that in both cases, the cusp in the absolute current curve (corresponding to a switch in polarity) is not observed at 0 V but is rather shifted from 0 V in a direction opposite to that of the voltage sweep. At -2 V (curve 1 in Figure 1), the negative current reaches a minimum value of ~-1 pA, and then it switches its polarity. Thus, contrary to expectation, the current leads the applied field, switching its polarity before that of the voltage, irrespective of the sweep direction. Furthermore, the curves indicate that the effect is symmetrical. This symmetry is observed not only in these MIM samples but also in similar measurements done on large-area MIS diodes.

We note that the contact stacks in the MIM structures are asymmetric with Ti (work function  $\Phi_m = 4.33 \text{ eV}$ ) on one side and Au ( $\Phi_m = 5.1 \text{ eV}$ ) on the other side. The asymmetry of the contacts is not reflected in the location of the cusp, but rather at the two ends of the sweep interval ( $\pm 5 \text{ V}$ ), where the current magnitude is inversely proportional to the energy barrier height at the metal/SiN interfaces. The work function of the SiN on SiO<sub>2</sub> substrate and with Si content ranging from 40% to 50% was shown to range from 4.28 eV to 4.22 eV, respectively.<sup>18</sup> Our SiN films contain a substantially smaller molar fraction of Si, as confirmed by the refractive index of the samples, averaging ~1.8 (Table II),

compared with the nominal value of 2.01 for stoichiometric Si<sub>3</sub>N<sub>4</sub> films. The SiN bandgap is thus increased.<sup>13</sup> Hence, the work function of our SiN also increases and might be higher than 4.28. Consequently, the Ti/SiN interface forms an electron ohmic contact since  $\Phi_{\text{SiN}} > \Phi_{\text{Ti}}$ , whereas the Au/SiN interface forms a Schottky contact since  $\Phi_{\text{SiN}} < \Phi_{\text{Au}}$ .

Despite the observed anomaly in the I-V behavior, the three SiN growth protocols used for samples A, B, and C yielded a notable reduction of gate leakage current of over two orders of magnitude in the negative biasing region, and of six orders of magnitude in the positive region as compared to the standard Schottky HFET (Figure 2).

In the interval from -2 V to 0 V (curve 1 in Figure 1), because the current and the external applied bias have opposite polarities, we can deduce that the shift in the current cusp must be due to an induced secondary displacement electric field in the dielectric, possibly originating from trapped space charge. This is supported by the observed symmetry, given that the initial bias point in the sweep interval ( $\pm 5 \text{ V}$  in Figure 1) is the same for both sweep directions. Even more compelling evidence is that the position of the shift approaches 0 V with decreasing initial bias.

We carry the analysis further by replotting the I-V curves using Eqs. (1) and (2) to identify the dominant conduction mechanisms in the region enclosing anomalous behavior. A linear fitting for any of these curves can be interpreted as demonstrating the existence of the respective current.<sup>14</sup>

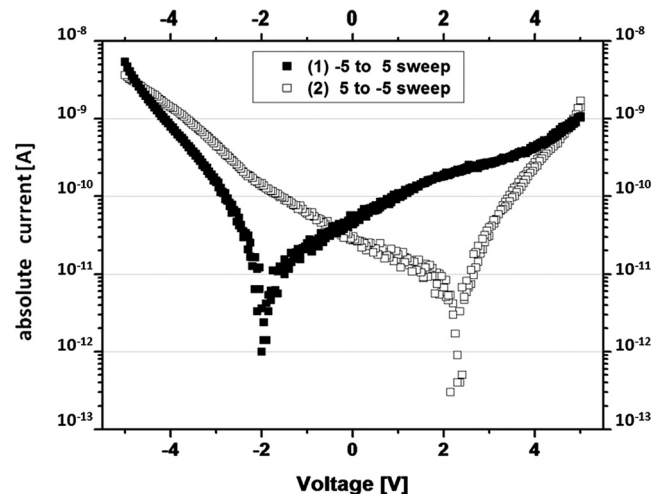


FIG. 1. Bi-directional voltage sweep for MIM sample #7, indicating a pronounced and symmetrical shift in both bias directions. The curves represent two separate measurements, not a hysteresis sweep.

TABLE II. SiN growth protocols for AlGaIn/GaN large-area diodes

Sample	RF power [W]	Temperature [°C]	Pressure [mTorr]	SiH <sub>4</sub> -NH <sub>3</sub> [sccm]	Thickness [nm]
A	45	350	650	36–29	12.9
B	15	350	250	17–50	11.5
C	15	250	650	17–50	12.4

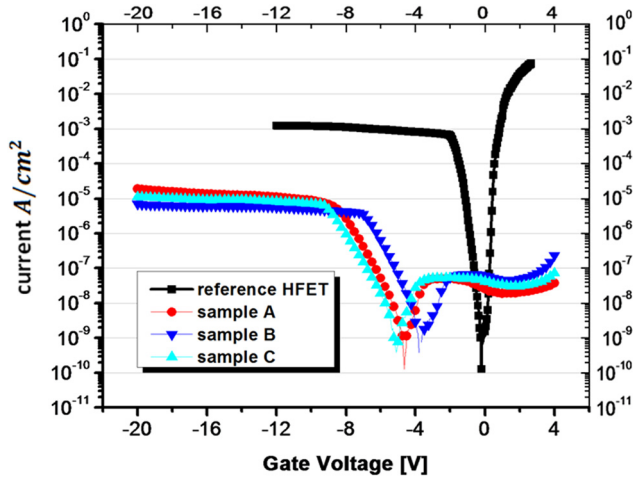


FIG. 2. MIS gate diode characteristics for samples A, B, and C, with the reference Schottky HFET measured by sweeping from the negative to the positive-bias region. The shift of the minimum is apparent in all samples except the reference HFET.

$$J_{PF} = qn_0\mu E_n \exp\left[-\frac{q}{kT}\left(\phi_B - \sqrt{\frac{qE_n}{\pi\epsilon_n}}\right)\right] \propto V \exp\left(2a\frac{\sqrt{V}}{T} - \frac{q\phi_B}{kT}\right) \quad (1)$$

$$J_{Schottky} = AT^2 \exp\left[-\frac{q}{kT}\left(\phi_B - \sqrt{\frac{qE_n}{4\pi\epsilon_n}}\right)\right] \propto T^2 \exp\left(a\frac{\sqrt{V}}{T} - \frac{q\phi_B}{kT}\right) \quad (2)$$

In Eq. (1),  $J_{PF}$  is the Poole-Frenkel current density,  $n_0$  is the carrier density,  $\mu$  is the effective carrier mobility,  $\Phi_B$  is the trap state depth,  $E_n$  is the applied electric field,  $q$  is the elementary charge,  $k$  is the Boltzmann constant, and  $T$  is the temperature. In Eq. (2),  $J_{Schottky}$  is the Schottky-type thermionic current density,  $A$  is the Richardson constant, and  $\Phi_B$  is the barrier height at the contact.

The corresponding data are shown in Figures 3 and 4 together with linear fits. In both graphs, the top arrow indicates

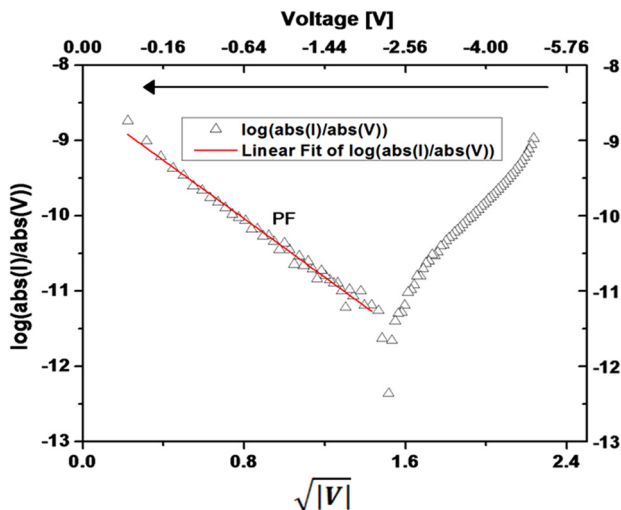


FIG. 3. Poole-Frenkel fitting in the negative-bias region. The current between  $-2$  V and  $0$  V shows a linear fit.

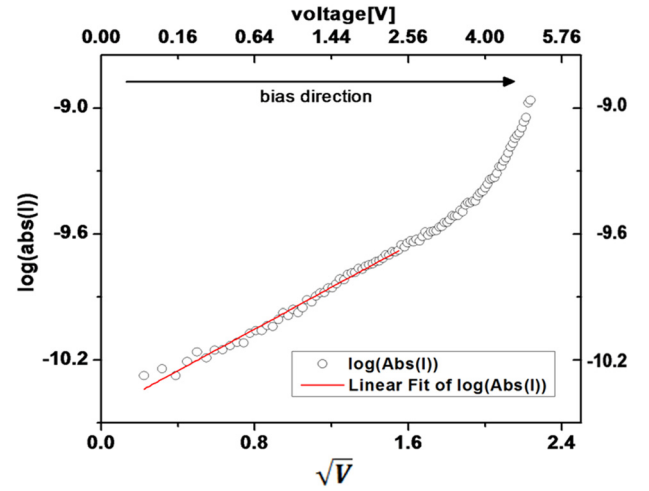


FIG. 4. Schottky-emission fitting in the positive-bias region. Schottky currents dominate at low fields.

the sweep direction. Figure 3 shows a PF fit at negative bias, whereas Figure 4 shows a Schottky fit at positive bias. In Figure 3, between  $-2$  V and  $0$  V a very good fit is observed, thereby suggesting that this is indeed a Poole-Frenkel current. In essence, the trapped space charge establishes an internal displacement field that biases nearby trap states and enhances the emission of trapped electrons and holes towards the conduction band and the valence band, respectively. Furthermore, when the external bias increases above  $0$  V, the space charge previously displaced by the negative bias will tend to return to its equilibrium state forced by the increasing positive external field. Essentially, this field causes the charge to diffuse across the length of the dielectric by hopping or to drift. In effect, the resultant internal potential diminishes and the PF current is then dominated by ohmic current. Similarly, Figure 4 shows the linear fit for the Schottky emission current in the positive-bias region. A good fit up to  $+3$  V is observed as well, thus implying that Schottky emission might contribute to the low-field current, in addition to ohmic currents.

Altogether, a good PF fit implies the existence of trapped space charge that produces an internal displacement electric field of opposite polarity to the external applied bias. The potential difference arises because of the gradient in the charge distribution. At the absolute current minima, the external voltage bias has decreased enough to match the internal potential induced by the charge distribution. At this point, both fields eliminate each other, leading to a quasi-saturation state similar to the initial state of thermal equilibrium, where the Fermi level is constant across the sample. Reducing the external potential even further, the internal displacement field induces current components of opposite polarity, which keeps increasing onwards with the addition of ohmic currents once the external potential crosses over to the other bias regime.

We also examined the correlation between the magnitudes of the observed minima shifts (voltage value that coincides with the cusp of the absolute current curve) in all MIM samples to the corresponding PECVD process parameters, using JMP statistical software. A reliable regression model as shown in Figure 5 exists. The shift in the minimum

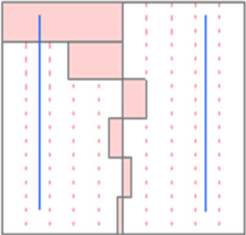
Term	Estimate	Std Error	t Ratio		Prob> t
Pressure*Ratio	-0.640625	0.034375	-18.64		0.0341*
Ratio(0.333, 1.25)	-0.284375	0.034375	-8.27		0.0766
Pressure(250,650)	0.121875	0.034375	3.55		0.1750
Temperature(250,350)	-0.071875	0.034375	-2.09		0.2840
Temperature*Ratio	0.040625	0.034375	1.18		0.4471
Temperature*Pressure	-0.028125	0.034375	-0.82		0.5635

FIG. 5. The JMP regression model. The large t-ratio of the first parameter indicates a strong correlation.

relative to 0 V is inversely proportional to the gas-flow ratio ( $\text{SiH}_4$  vs.  $\text{NH}_3$  gas flow). However, the shift is also inversely proportional to the combination of the pressure and the gas-flow ratio. The dependency is stronger and statistically more significant in the latter case, as indicated by the greater t-ratio which is large enough to prove the effect to be statistically relevant.<sup>19</sup> The regression model is thus very accurate and the gas-flow ratio and the pressure, both individually and in combination, strongly affect the magnitude of the shift.

At a deposition power of 15 W, the gas-flow ratio, and/or pressure-ratio combined reduce the voltage shift. Defects in SiN, such as Si-Si bonds, demonstrably produce trap states in the middle of the bandgap, whereas Si dangling bonds produce states within the vicinity of the conduction band.<sup>20,21</sup> Both kinds of defects if coordinated with hydrogen impurities, can be shifted deeper into the band gap and consequently contribute to trapping. Notably, non-stoichiometric SiN can contain large amounts of atomic hydrogen.<sup>14</sup> Higher pressure increases the collision cross section and accelerates the dissociative ionization of the precursor gases, thereby allowing the incomplete synthesis of SiN.<sup>21</sup> This might introduce more broken bonds and therefore traps. Hence, the combination of higher pressure and higher silane gas flow would reduce the minima shift, possibly by eliminating a portion of atomic hydrogen and thus producing a more complete synthesis reaction by mediating the formation of Si dangling bonds and/or Si-Si bonds. A higher quality SiN film manifesting a reduced minima shift is desirable for reliable and low power FET operation whereby the dielectric capacitance is reduced, the voltage drop across the dielectric is as small as possible and the device threshold voltage is closer to zero. This quality akin to a memory-like or a hysteresis-like behavior can be tailored for creating interesting devices. It can be employed to avoid unwanted rapid switching in sensitive circuits due to noise generated from electronic components in high temperature environment. The two current minima (Figure 1) can define a hysteresis loop of the device, simulating the two threshold limits of a Schmitt trigger.

We conclude that the current opposite to the applied external electric field is caused by internal space charge formation inside the SiN films, forming an internal electrical field that enhances the Poole Frenkel current mechanism and/or Schottky emission from contacts. Additionally, we find that the combination of higher pressure and higher silane gas flow during PECVD SiN deposition reduces the value of the zero shift, by possibly eliminating a portion of atomic hydrogen and thus carrying the whole synthesis reaction more completely by mediating the formation of Si dangling

bonds and/or Si-Si bonds. Finally, we have reported a promising reduction of gate leakage current by several orders of magnitude by using the SiN as gate dielectric in large area AlGaN/GaN diodes.

- <sup>1</sup>M. Marso, G. Heidelberger, K. M. Indlekofer, J. Bernat, A. Fox, P. Kordos, and H. Lueth, *IEEE Trans. Electron Devices* **53**, 1517–1523 (2006).
- <sup>2</sup>S. Saygi, A. Koudymov, V. Adivarahan, J. Yang, G. Simin, M. Asif Khan, J. Deng, R. Gaska, and M. S. Shur, *Appl. Phys. Lett.* **87**, 043505 (2005).
- <sup>3</sup>M. A. Khan, G. Simin, J. W. Yang, J. P. Zhang, A. Koudymov, M. S. Shur, R. Gaska, X. H. Hu, and A. Tarakji, *IEEE Trans. Microwave Theory Tech.* **51**, 624–633 (2003).
- <sup>4</sup>D. Gregusova, R. Stoklas, K. Cico, T. Lalinsky, and P. Kordos, *Semicond. Sci. Technol.* **22**, 947–951 (2007).
- <sup>5</sup>M. Eickelkamp, D. Fahle, J. Lindner, M. Heuken, C. Lautensack, A. Noculak, H. Kalisch, R. H. Jansen, and A. Vescan, in 33rd European Workshop on Compound Semiconductors and Integrated Circuits (WOCSDICE 2009), Malaga, Spain, May 2009.
- <sup>6</sup>C. Liu, E. F. Chor, and L. S. Tan, *Semicond. Sci. Technol.* **22**, 522–527 (2007).
- <sup>7</sup>R. N. Wang, Y. Cai, C. W. Tang, K. M. Lau, and K. J. Chen, *IEEE Electron Device Lett.* **27**, 793–795 (2006).
- <sup>8</sup>M. Ochiai, M. Akita, Y. Ohno, S. Kishimoto, K. Maezawa, and T. Mizutani, *Jpn. J. Appl. Phys. Part 1* **42**, 2278–2280 (2003).
- <sup>9</sup>T. Hashizume, S. Ootomo, T. Inagaki, and H. Hasegawa, *J. Vac. Sci. Technol. B* **21**(4), 1828–1838 (2003).
- <sup>10</sup>M. Jo, H. Park, M. Chang, H.-S. Jung, J.-H. Lee, and H. Hwang, *Microelectron. Eng.* **84**(9–10), 1934–1937 (2007).
- <sup>11</sup>S. Ponce-Alcantra, C. Del Canizo, J. Hofstetter, and A. Luque, in Spanish Conference on Electron Devices, Madrid, Spain, 31 January–2 February 2007.
- <sup>12</sup>M. Tao, D. Park, S. N. Mohammad, D. Li, A. E. Botchkerv, and H. Morkoc, *Philos. Mag. B* **73**(4), 723–736 (1996).
- <sup>13</sup>H. Sato, H. Kato, Y. Ohki, K. S. Seol, and T. Noma, in Proceedings of 2001 International Symposium on Electrical Insulating Materials (ISEIM 2001), Himeji, Japan, 19–22 November 2001.
- <sup>14</sup>C.-C. Lu, C.-L. Ho, M.-C. Wu, T.-T. Shi, and W.-J. Ho, *IEEE Trans. Dielectr. Electr. Insul.* **8**(6), 1011–1015 (2001).
- <sup>15</sup>H. Campbell, P. S. Davids, D. L. Smith, N. N. Barashkov, and J. P. Ferraris, *Appl. Phys. Lett.* **72**, 1863 (1998).
- <sup>16</sup>M. J. Anderson and P. J. Whitcomb, “Design of Experiments,” in *Kirk-Othmer Encyclopedia of Chemical Technology* (Wiley, 2010), pp. 1–22, DOI: 10.1002/0471238961.0405190908010814.a01.pub3.
- <sup>17</sup>M. Eickelkamp, M. Hanna, M. Brast, N. Ketteniss, H. Kalisch, R. H. Jansen, and A. Vescan, in 34th European Workshop on Compound Semiconductors and Integrated Circuits (WOCSDICE 2010), Darmstadt/Seeheim, Germany, 17–19 May 2010.
- <sup>18</sup>H. C. Wen, H. N. Alshareef, H. Luan, K. Choi, P. Lysaght, H. R. HarrisHaHa, C. Huffman, G. A. Brown, G. Bersuker, P. Zeitsoff, H. Huff, P. Majhi, and B. H. Lee, *Dig. Tech. Pap. - Symp. VLSI Technol.* **2005**, 46–47.
- <sup>19</sup>G. E. P. Box, W. G. Hunter, and J. S. Hunter, *Statistics for Experimenters* (Wiley, New York, 1978).
- <sup>20</sup>G. Lucovsky and S. Y. Lin, *J. Vac. Sci. Technol. B* **3**(4), 1122–1128 (1985).
- <sup>21</sup>S.-S. Han, L. Cai, G. S. May, and A. Rohatgi, *IEEE Trans. Semicond. Manuf.* **9**(3), 303–311 (1996).